Electronic Supplementary Information

for

A force field for tricalcium aluminate to characterize surface properties, initial hydration, and organically modified interfaces in atomic resolution

by

Ratan K. Mishra,[1] Lucia Fernández-Carrasco,[2] Robert J. Flatt,[1*] and Hendrik Heinz[3*]

[1] Department of Civil, Environmental and Geomatic Engineering, ETH Zurich, CH-8093 Zürich, Switzerland

[2] Department of Architectural Technology I, Universitat Politècnica de Catalunya, 08028 Barcelona, Spain

[3] Department of Polymer Engineering, University of Akron, Akron, OH 44325, USA

[*] Corresponding authors: flattr@ethz.ch, hendrik.heinz@uakron.edu

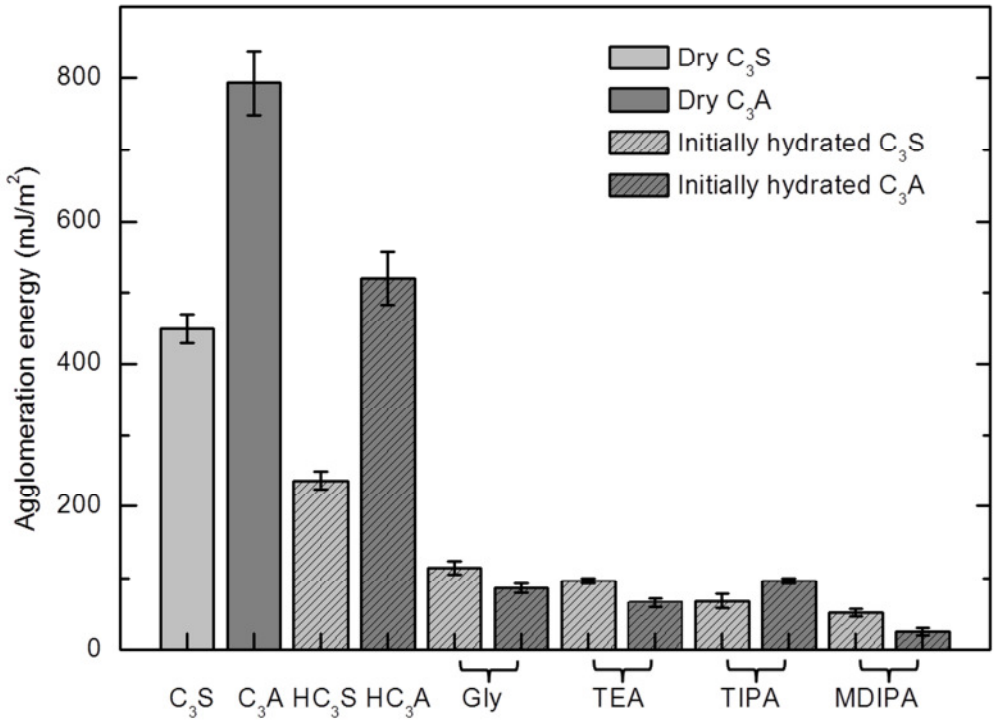

Figure S1. Agglomeration energy of tricalcium silicate (C_3S, from ref. [1]) and tricalcium aluminate (C_3A) surfaces at 363 K, including dry, hydrated, and organically modified surfaces. The dosage of organics is 0.20 mg/m^2, equivalent to 130% of a molecular monolayer between two surfaces.

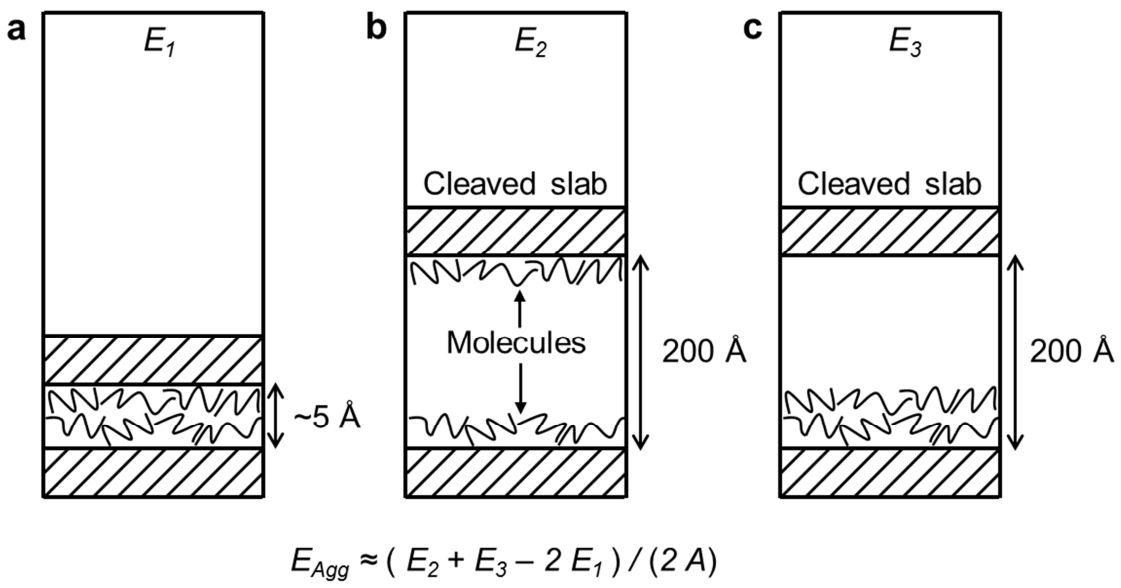

Figure S2. Schematic of the calculation of agglomeration energies E_{Agg} under periodic boundary condition using molecular dynamics simulation in the *NVT* ensemble (not drawn to scale). (a) Unified surfaces. (b, c) Separated surfaces. The agglomeration energy between two surfaces depends on the distribution of organic additives between the separated surfaces that may range from equal (b) to one-sided (c). *E* represents the total energy of the system and *A* the cross-sectional area of one surface.

Table S1. Coverage of cleaved surfaces with alcohols in experiment and simulation. The chosen values correspond to 500 g of a 40% concentrated aqueous solution of alcohols per ton of cement with a specific particle surface area of 1 m^2/g.

System	Dosage (mg/m^2)	Surface area in model (nm^2)	No. of Molecules
C_3A-TIPA	0.20	9.32	6
C_3A-TEA	0.21	9.32	8
C_3A-MDIPA	0.21	9.32	8
C_3A-Gly	0.20	9.32	12

S1. Computational Details

In this section, the molecular models, energy expressions, simulation protocols, uncertainties, and limitations are described.

S1.1. Molecular Models. We employed X-ray data from Mondal and Jeffery[2] to construct a 3D periodic model of a unit cell of $Ca_3Al_2O_6$. The space group of the cubic unit cell is *Pa*3 with a lattice parameter of 1.5263 nm (Figure 1). Various multiples of the C_3A unit cell were employed for the calculation of cell parameters, thermal expansion, mechanical properties, vibration properties, cleavage energies, and agglomeration energies with organic compounds as described in detail below. Models of the surfaces were prepared by cleavage and cation relaxation using temperature gradient molecular dynamics (Figure 6).[3] Models of the organic molecules were built using the graphical user interface of Materials Studio (Scheme 3).[4]

S1.2. Energy Expression. We employed the PCFF version of the force field for all data reported, unless specifically indicated for comparison. The use of the parameters within slightly different types of force fields (CFF/PCFF/COMPASS, CHARMM, AMBER, CVFF, OPLS-AA) introduces small, mathematically inevitable differences in structures and energies. These differences are typically smaller than the uncertainty in experimental measurements (Table 5, section 3.4), and also insignificant in comparison to the performance of various density functionals on a local scale.

S1.3. Lattice Constants and Thermal Expansion. For the validation of lattice constants in NPT molecular dynamics, we employed a 2×2×2 supercell of 3.0526 × 3.0526 × 3.0526 nm^3 dimension. The quality of fit of lattice parameters and bonded

parameters of the aluminate rings remains the same for larger unit cells or for a 1×1×1 unit cell (shown for in Table 3).

For the optimization of the force field parameters, more than one thousand molecular mechanics minimizations and molecular dynamics simulations using different test sets of parameters were carried out. The final validation of lattice parameters (*a, b, c, α, β, γ*) involved molecular dynamics simulation in the NPT ensemble for 50 ps for equilibration and 200 ps for sampling of averages using the Discover program.[4] We employed the Verlet integrator, velocity scaling (preferred) and the Andersen thermostat for temperature control,[5] as well as pressure control by the Parrinello-Rahman method.[6] The time step was 0.5 fs (smaller than the usual 1 fs) to enable pressure control in high precision. Further, we employed a spherical cutoff of van der Waals interactions at 1.2 nm, Ewald summation of Coulomb interactions with a high accuracy of 10^{-6} kcal/mol, a temperature of 298.15 K, and a pressure of 0.0001 GPa. Computed lattice parameters and density remained constant for simulation times beyond tens of nanoseconds.

For the analysis of thermal expansion (Figure 3), several simulations were employed with different temperature settings ranging from 300 K to 800 K using otherwise identical protocol.

S1.4. Mechanical Properties. We employed super cells of dimensions of 3.0526 × 3.0526 × 3.0526 nm^3 to compute volume compression, bulk modulus, Young's modulus, and Poisson ratios (Figure 4, Tables 3 and 5).

The computation of volume compression and bulk modulus *K* involved energy minimization of the crystal structure, followed by a series of NPT molecular dynamics simulations for 200 ps at ambient temperature for different pressure settings

(corresponding to compressive triaxial stress). The first pressure setting was ambient pressure to relax the crystal and obtain exact average cell parameters as in the computation of cell parameters. Then, the compressive triaxial stress σ was varied from 0.1 GPa to 8.0 GPa in additional simulations and changes in cell volume $V = a^3$ were recorded (Figure 4a, Tables 4 and 5). The bulk modulus K was calculated from the slope of the compression curve locally near each pressure setting:

$$K = -V \frac{\partial \sigma}{\partial V}. \tag{3}$$

The protocol for molecular dynamics simulation was the same as in the optimization of the cell parameters, except for the different stress tensors employed.

The computation of Young's moduli and the Poisson ratio involved a series of NPT molecular dynamics simulations with increasing uniaxial stress in the three coordinate directions (σ_{xx}, σ_{yy}, and σ_{zz}). Several stress settings in the range 0.00 GPa to 2.0 GPa were chosen and individual NPT calculations performed for 200 ps. The uniaxial stresses and resulting strains (ε_{xx}, ε_{yy}, and ε_{zz}) were plotted as three independent stress-strain curves (Figure 4b). Young's modulus was obtained as the average slope (Table 4):

$$E_x = \partial \sigma_{xx} / \partial \varepsilon_{xx}. \tag{4}$$

The Poisson ratio was obtained as the average ratio between expansion strain in the direction orthogonal to the applied compressive uniaxial stress and the compressive strain in the direction of uniaxial stress, for example, $\nu = -\varepsilon_{yy} / \varepsilon_{xx} = -\varepsilon_{zz} / \varepsilon_{xx}$ for compressive uniaxial stress in x direction. The Young's moduli E_x, E_y, and E_z in the x, y, and z directions are equal and only one Poisson ratio is reported due to isotropic crystal symmetry of C_3A. Simulation protocols equaled those used in the computation of unit

cell parameters. Separate stress-strain calculations for all principal axes helped refine estimates of the uncertainty. In all stress-strain simulations, the fluctuation of the instantaneous stress from the average value was typically ±0.3 GPa independent of the chosen target stress. The statistical uncertainty of the average was significantly lower as is indicated by corresponding error bars of bulk modulus (Figure 4a) and stress (Figure 4 b).

S1.5. Vibration Spectra. Vibration spectra of C_3A (Figure 5) were calculated using a pre-equilibrated model of the unit cell. Molecular dynamics simulation in either NVT or NPT ensemble was carried out for 20 ps with a time step of 1 fs and collection of snapshots every 1 fs. The velocity autocorrelation function (VACF) was then calculated for all atoms using the collected snapshots (trajectory), and the Fourier transform of the VACF yielded the vibration spectrum.[4] The computed vibration spectrum corresponds to the superposition of Raman and IR spectra since the force field does not apply selection rules.

It has been mentioned in the main text that the experimentally observed frequencies of bending vibrations of Al–O–Al and O–Al–O angles in the range 550 to 300 cm^{-1} are shifted by approximately +100 cm^{-1} in molecular dynamics simulation. These angle bands are represented by the force constant $K_{\theta,ijk}$ of 110 kcal/(mol·rad^2) (Figure 5 and Table 1). A better fit between computed bending frequencies and measurements can be obtained using a smaller value of $K_{\theta,ijk}$ of ~85 kcal/(mol·rad^2) although some bond angles (especially the wide Al-O-Al angle) would then deviate more from experiment and the conformational flexibility of the aluminate rings would increase relative to experiment, showing some artificial “floppiness”. These limitations are owed to the

approximation of the balance of covalent and ionic bonding by bonded terms and nonbonded terms in the force field. First, covalent bonds are only partial as in C_3A and still represented by full covalent terms. Second, exclusion conventions of nonbond interactions between 1,2 and 1,3 bonded are applied that become increasingly unnecessary as ionic contributions to bonding dominate. These two conventions cause the observed imperfection while they lead to simplicity and broad applicability of harmonic force fields to organic molecules and inorganic compounds. It can be imagined that such conventions could be locally changed for certain compounds such as C_3A, accompanied by appropriate changes in parameters, to reflect the true chemistry better. To date, uncertainties of this order of magnitude in vibration frequencies are not unusual in force fields and even in DFT calculations for inorganic compounds. If, in addition, thermodynamic consistency is not observed, discrepancies of much larger scale up to structural instability and need for fixed atoms are known.[7, 8]

S1.6. Cleavage Energy. For the computation of cleavage and agglomeration energies, we examined various Miller planes, i.e., (100), (010), (001), (200), (020), and (002), that are identical due to cubic symmetry. The calculation of the cleavage energy involved the simulation of the mineral slabs in separated and in unified arrangements (Figure 6).[1, 3, 9] The cleavage energy was calculated as the difference in average energy of two separated (cleaved) surfaces in equilibrium (Figure 6c) and the corresponding homogeneous mineral slab (Figure 6a):

$$E_{cleavage} = \frac{E_{separated} - E_{unified}}{2A}. \quad (5)$$

We employed a (2×4×2) super cell of ~3×6×3 nm^3 volume to model cleavage of the (010) plane under 3D periodic boundary condition. The simulation cell of the unified

mineral slab was extended in the *y* direction to a length of 50 nm to avoid interactions with its own periodic image. Models of the cleaved surfaces were constructed by separation of the (010) surface plane by 20 nm, retention of the conformation of the aluminate rings and the position of inner calcium ions, as well as equal distribution of cations on both surfaces to minimize local electric fields. Subsequently, the two created surfaces were relaxed by temperature gradient MD (Figure 6b,c).[1, 3, 9] In this procedure, only the ions directly on top of both surfaces were mobile and all other atoms were fixed. The NVT ensemble was employed over a period of 20 ps, starting with an initial temperature of 10000 K that converts to a final temperature of 298.15 K using the Berendsen thermostat with a decay constant (half-life) of 1 ps. This protocol allows vertical and lateral movement of the ions on the two created surfaces to identify energetically preferred positions. Convergence to lowest energy was tested by energy minimization of several snapshots along the trajectory, as well as by repetitions of the procedure (usually not needed). Convergence to the same energy basin occurred within few kcal/mol, i.e., <10 mJ/m^2 deviation.

As a next step in the computation of cleavage energies, models of the relaxed unified and relaxed separated surface slabs were subjected to NVT molecular dynamics for 4 to 6 ns with a time step of 1 fs, temperatures of 298.15 K and 363.15 K, Ewald summation of Coulomb interactions with accuracy of 10^{-6} kcal/mol, and data collection at every 200 fs. The first half of the trajectory (2 ns) served the equilibration of the structure and was discarded. The last 2 ns served for recording snapshots and thermodynamic data to determine the average energies and uncertainties using block averages over major portions of the trajectory (Table 6).

S1.7. Superficially Hydrated Surfaces. Models of the superficially hydrated (010) C_3A surfaces were prepared by assuming the initial hydration reaction described in section 4.2 (Figure 7). The stoichiometric conversion of aluminate group into aluminol groups, addition of hydroxide ions, and new positioning of Ca^{2+} ions was implemented using the graphical user interface of Materials Studio.[4] Modified charges and force field types were assigned accordingly. Subsequently, we carried out temperature gradient molecular dynamics to relax the newly created surface layers (see above). In this procedure, atomic positions underneath the surface layers were fixed. All atoms were again mobile in follow-on simulations at the target temperature.

S1.8. Agglomeration Energy. The calculation of agglomeration energies of the pure, hydrated, as well as organically modified hydrated surfaces was carried out using relaxed models of cleaved and unified surfaces, similar as in the calculation of cleavage energies (see also ref. [1]). In the presence of organic thin films, the calculation of agglomeration energies involved three independent calculations for the same system with different initial distribution of the organic molecules on the surfaces to obtain better staistics and verify convergence. Each independent calculation involved three simulation boxes with the molecules distributed on both cleaved surfaces, on one of the cleaved surfaces only, and of the two surfaces joined together (Figure S2). These models were of the same dimension and composition, and subjected to NVT molecular dynamics simulation at 363 K. A total simulation time of 3 ns was chosen for each individual simulation, consisting of 400 ps initial equilibration at 363.15 K temperature, 200 ps annealing at 600 K, 800 ps further equilibration at 363.15 K, and 1 ns for recording thermodynamic quantities and snapshots every 300 fs at 363.15 K. Annealing at 600 K was necessary to identify global

energy minima of the surfaces in all states, i.e., the pure cleaved surfaces and agglomerated surfaces, the hydrated cleaved and agglomerated surfaces with amorphous calcium hydroxide layers, as well as the hydrated cleaved and agglomerated surfaces containing adsorbed organic molecules. In the presence of adsorbed alcohols, the molecules would detach from the surface upon annealing and were placed back onto the surface before continuation of the remaining simulation protocol.

The surface coverage with alcohol molecules in the simulation was chosen corresponding to a typical dosage of grinding additives of 500 g solution per ton of cement with a concentration of 40% organic molecules by mass, and assuming a specific surface area of cement particles of 1.0 m^2/g determined by the BET method.[1, 10]

S1.9. Limitations and Opportunities. The current models focus on pure C_3A, however, extensions to well-known impure solid solutions and other polymorphs of C_3A[2, 11-13] are feasible. Common impurities include the replacement of Al^{3+} by Fe^{3+} and Si^{4+} ions, as well as substitution of Ca^{2+} by Na^+, K^+, and Mg^{2+} in the low percent range. Up to a limit of about 1% Na_2O in $Na_{2x}Ca_{3-x}Al_2O_6$, for example, the crystal structure remains the same, and the cubic crystal system changes into orthorhombic or monoclinic for higher amounts. The C_3A force field can be applied to such variable compositions using parameters for common impurities (cations, silicate, octahedral aluminate) in the INTERFACE force field.[14] The relative stability of structural defects and their distributions can be assessed by comparisons of the energy upon equilibration by molecular dynamics. While some ambiguity in preferred structures and loss in performance may occur, predictions likely remain quantitative to semi-quantitative.

The hydration reaction of C_3A is difficult to control experimentally and accordingly many models for consecutive hydration stages may be investigated. The focus in this work is on the earliest stage in the hydration process. Models with hydrolyzed ring structures and aqueous $[Al(OH)_{3+n}(H_2O)_{3-n}]^{n-}$ complexes in later stages (Scheme 2) can also be represented by this model and by using additional parameters for aluminate in ettringite and monosulfate.[14]

Extensions for polarizability in different environments and for chemical reactions, e.g. Morse potentials, could widen the applicability of the force field. Partial atomic charges have a remaining uncertainty up to ±0.1e, and thus leave a small margin of uncertainty in computed cleavage and adsorption energies. Specifically, the Ca^{2+} ion can have a flexible charge depending on the hydration state (+1.5e in the solid, up to +2.0 in water). Such effects can be taken into account by parameter adjustments during dissolution processes, while it is advantageous to introduce only few additional parameters. The direct simulation of chemical reactions may be best achieved by DFT methods on a local scale. On a scale larger than 1 to 2 nm, it may be preferable to investigate a number of key stages along the reaction coordinate with adjusted bond settings of the force field, similar to the models of the initial hydration stages. Further force field types and parameters for intermediates and transition states can be added if needed.

Supporting References

1. R. K. Mishra, R. J. Flatt and H. Heinz, *J. Phys. Chem. C*, 2013, 117, 10417-10432.
2. P. Mondal and J. W. Jeffery, *Acta Cryst. B-Struct. Sci.*, 1975, 31, 689-697.
3. Y. T. Fu and H. Heinz, *Chem. Mater.*, 2010, 22, 1595-1605.
4. *Materials Studio 6.0 Program Suite and User Guide*, Accelrys, Inc., 2012.
5. H. C. Andersen, *J. Chem. Phys.*, 1980, 72, 2384-2393.
6. M. Parrinello and A. Rahman, *J. Appl. Phys.*, 1981, 52, 7182-7190.
7. H. Heinz, H. Koerner, K. L. Anderson, R. A. Vaia and B. L. Farmer, *Chem. Mater.*, 2005, 17, 5658-5669.
8. S. H. Garofalini, *J. Chem. Phys.*, 1982, 76, 3189-3192.
9. H. Heinz, R. A. Vaia and B. L. Farmer, *J. Chem. Phys.*, 2006, 124, 224713.
10. S. Brunauer, P. H. Emmett and E. Teller, *J. Am. Chem. Soc.*, 1938, 60, 309-319.
11. H. F. W. Taylor, *Cement Chemistry*, Academic Press, London, 1997.
12. K. Fukuda, S. Inoue and H. Yoshida, *J. Am. Ceram. Soc.*, 2003, 86, 112-114.
13. F. C. Lee, H. M. Banda and F. P. Glasser, *Cem. Concr. Res.*, 1982, 12, 237-246.
14. H. Heinz, T.-J. Lin, R. K. Mishra and F. S. Emami, *Langmuir*, 2013, 29, 1754-1765.